

## A 0.12mm<sup>2</sup> Wien-Bridge Temperature Sensor with 0.1°C (3σ) Inaccuracy from -40°C to 180°C

Pan, Sining; Gürleyük, Çağrı; Pimenta, Matheus F.; Makinwa, Kofi A.A.

**DOI**

[10.1109/ISSCC.2019.8662457](https://doi.org/10.1109/ISSCC.2019.8662457)

**Publication date**

2019

**Document Version**

Final published version

**Published in**

2019 IEEE International Solid-State Circuits Conference, ISSCC 2019

**Citation (APA)**

Pan, S., Gürleyük, Ç., Pimenta, M. F., & Makinwa, K. A. A. (2019). A 0.12mm<sup>2</sup> Wien-Bridge Temperature Sensor with 0.1°C (3σ) Inaccuracy from -40°C to 180°C. In J. van der Spiegel (Ed.), *2019 IEEE International Solid-State Circuits Conference, ISSCC 2019* (Vol. 2019-February, pp. 184-186). Article 8662457 IEEE. <https://doi.org/10.1109/ISSCC.2019.8662457>

**Important note**

To cite this publication, please use the final published version (if applicable). Please check the document version above.

**Copyright**

Other than for strictly personal use, it is not permitted to download, forward or distribute the text or part of it, without the consent of the author(s) and/or copyright holder(s), unless the work is under an open content license such as Creative Commons.

**Takedown policy**

Please contact us and provide details if you believe this document breaches copyrights. We will remove access to the work immediately and investigate your claim.

***Green Open Access added to TU Delft Institutional Repository***

***'You share, we take care!' - Taverne project***

**<https://www.openaccess.nl/en/you-share-we-take-care>**

Otherwise as indicated in the copyright section: the publisher is the copyright holder of this work and the author uses the Dutch legislation to make this work public.

### 10.3 A 0.12mm<sup>2</sup> Wien-Bridge Temperature Sensor with 0.1°C (3 $\sigma$ ) Inaccuracy from -40°C to 180°C

Sining Pan, Çağrı Gürleyük, Matheus F. Pimenta, Kofi A. A. Makinwa

Delft University of Technology, Delft, The Netherlands

Resistor-based temperature sensors can achieve much higher resolution and energy efficiency than conventional BJT-based sensors [1], but they typically occupy more area (>0.25mm<sup>2</sup>) and have lower operating temperatures ( $\leq 125^\circ\text{C}$ ) [2-4]. This work describes a 0.12mm<sup>2</sup> resistor-based sensor that uses a Wien-bridge (WB) filter to achieve 0.1°C (3 $\sigma$ ) inaccuracy from -40°C to 180°C. Compared to a state-of-the-art WB sensor [4], it occupies 6 $\times$  less area and achieves comparable relative accuracy over a 76% wider operating range.

As shown in Fig. 10.3.1, the heart of the sensor is a Wien Bridge (WB) bandpass filter made from polysilicon resistors ( $R_{WB} = 64\text{k}\Omega$ ) and MIM capacitors ( $C_{WB} = 5\text{pF}$ ). Unlike Wheatstone-bridge sensors [2,3], WB sensors only require one type of resistor, resulting in higher accuracy, and facilitating the experimental characterization of undocumented resistor properties such as  $1/f$  noise and stress sensitivity. The filter is driven by a fixed-frequency square wave ( $f_{drive} = 500\text{kHz}$ ) so that its temperature-dependent phase-shift  $\phi_{WB}$  can be digitized by a phase-domain delta-sigma modulator (PD $\Delta$  $\Sigma$ M) [3]. In the PD $\Delta$  $\Sigma$ M, phase detection is performed by a chopper in the feedback loop of the 1<sup>st</sup> integrator (Fig. 10.3.2). Depending on the state of the bitstream BS, the chopper is driven by one of two reference phases  $\phi_{0,1}$  ( $90^\circ \pm 30^\circ$  w.r.t. to the phase of  $f_{drive}$ ) such that the DC component of the integrated current is either positive or negative. The integration capacitor  $C_{int}$  must then be dimensioned to filter out the resulting ripple and ensure that the output of the 1<sup>st</sup> integrator does not clip. In [4], this required a 180pF capacitor that occupied more than half of the sensor's area.

To reduce the size of  $C_{int}$ ,  $R_{WB}$  can be increased, but this will be at the expense of worse resolution. A better approach is to increase the output swing of the 1<sup>st</sup> integrator. In this work, the 1<sup>st</sup> integrator is built around a two-stage Miller-compensated opamp based on current-reuse amplifiers (Fig. 10.3.2). The 1<sup>st</sup> stage provides good energy efficiency, while the 2<sup>nd</sup> uses high- $V_T$  devices to efficiently provide a near rail-to-rail output swing. Compared to the conventional choice of two common-source stages, the second stage provides twice the output current for the same bias current. Together with the doubling of  $R_{WB}$ , this allows the value of  $C_{int}$  to be reduced from the 180pF used in [4], to 23pF. At room temperature (RT), the amplifier draws 14 $\mu\text{A}$  and has a gain bandwidth product of 17MHz. To further reduce area, the 2<sup>nd</sup> integrator and the feed-forward coefficient are realized in a switched-capacitor manner, thus avoiding the large resistors used in [4]. The associated folded-cascode amplifier draws only 2.5 $\mu\text{A}$  at RT. On-chip logic generates the drive signal  $f_{ref}$  and the phase references  $\phi_{0,1}$  from an external 6MHz frequency reference.

However, reducing  $C_{int}$  will increase the opamp's closed-loop input impedance  $Z_{in}$  ( $\propto 1/(C_{int} \cdot \text{GBW})$ ). This is in series with the WB and is thus a source of spread and  $1/f$  noise. To minimize spread, a constant-Gm biasing circuit based on a resistor of the same type as  $R_{WB}$  ensures that  $Z_{in}$  tracks  $R_{WB}$  over a wide temperature range. Although the opamp is effectively chopped, the  $1/f$  noise present in its bias current will modulate  $Z_{in}$ , and thus  $R_{WB}$ , causing residual  $1/f$  noise. To minimize this, the core of the biasing circuit was realized with large PMOS devices ( $W/L = 40\mu\text{m}/5.5\mu\text{m}$ ), and critical current mirrors were realized with the standard NPN transistors available in the chosen process (Fig. 10.3.2). Simulations show that the  $1/f$  corner of the sensor is then about 1Hz and that  $R_{WB}$  is less than 1% of  $Z_{in}$  over corners.

Three pairs of identical sensors based on silicided p-poly (SP), unsilicided n-poly (NP) and high-resistive poly (HRP) resistors were fabricated on the same die in a 0.18 $\mu\text{m}$  CMOS process (Fig. 10.3.7). This facilitates the use of differential measurements to distinguish sensor drift from the inevitable ambient temperature drift. Each sensor consumes 29 $\mu\text{A}$  from a single 1.8V supply and occupies 0.12mm<sup>2</sup>, of which the WB occupies 25%. PSDs of the bitstream outputs of the three sensors are shown in Fig. 10.3.3 (top) based on differential data captured during a 100s measurement interval. Figure 10.3.3 (bottom) shows the calculated resolution of each sensor versus conversion time. Due to its greater temperature coefficient (TC), the SP sensor exhibits the best resolution: 460 $\mu\text{K}$  in a 10ms conversion time, corresponding to a 110fJ/K<sup>2</sup> resolution FoM. For longer

conversion times, sensor resolution is limited by  $1/f$  noise. The corner frequencies are  $\sim 4\text{Hz}$  (NP and HRP), and  $\sim 1\text{Hz}$  (SP). However, the SP corner frequency is limited by the readout electronics.

10 chips (60 sensors) from a single batch were packaged in ceramic DIL and characterized from -40°C to 180°C. To correct for the inherent cosine nonlinearity of the PD $\Delta$  $\Sigma$ M and the non-linear relationship between  $\phi_{WB}$  and  $R_{WB}$  (Fig. 10.3.1, bottom), a 7<sup>th</sup>-order polynomial is used to translate the decimated output of each sensor into an equivalent sensor resistance  $R_{WB}$ . Since the temperature dependency of polysilicon resistors is comparatively linear, this approach minimizes the residual error after a 1<sup>st</sup>-order fit [4]. Figure 10.3.4 (top) shows the resulting temperature dependence of each resistor type. The following RT TCs were extracted: 0.31%/°C (SP), -0.15%/°C (NP) and -0.10%/°C (HRP), which agree with the process documentation. After a 1<sup>st</sup>-order fit to compensate for process spread, followed by the use of a fixed 6<sup>th</sup>-order polynomial to correct for the systematic non-linearity of the sensors, their residual spread is shown in Fig. 10.3.4 (bottom). The sensors achieve 3 $\sigma$  inaccuracies of 0.1°C (SP), 0.4°C (NP) and 0.9°C (HRP) from -40°C to 180°C. After a correlated 1-point trim [3], the SP sensor achieves an inaccuracy of 0.4°C (3 $\sigma$ ), which is comparable with that of BJT-based sensors [5].

To observe the effects of mechanical stress, 10 chips from the same batch were characterized in injection-molded plastic QFN packages. Figure 10.3.5 (top) shows the average dependency of  $R_{WB}$  for both the ceramic and plastic packaged chips. After using the same non-linearity correction polynomials determined for the ceramic packaged chips, the inaccuracy after a 1<sup>st</sup>-order fit increases by only 0.2°C for the SP sensors, but to 1.4°C for the NP sensors, and even 2.5°C for the HRP sensors (Fig. 10.3.5 (bottom)). The sharp inflexion in all the inaccuracy plots around 100°C is probably due to the effects of moisture on the plastic packages [7]. Of the three resistor types, the SP resistor is clearly the least stress sensitive, exhibiting a packaging shift similar to that of BJT-based sensors [6].

In Fig. 10.3.6 the performance of the SP sensor is summarized and compared to the state-of-the-art. Compared to a state-of-the-art WB sensor [4], this design has a 76% larger operating range and occupies 6 $\times$  less area. The latter is achieved at the expense of somewhat less relative inaccuracy [1]. Compared to a state-of-the-art WhB sensor [3], it achieves better accuracy and occupies 2 $\times$  less area, but is less energy efficient. Measurements in plastic packages show that the SP sensors are quite insensitive to packaging stress ( $< 0.2^\circ\text{C}$  packaging shift) and obtain good accuracy after a 1-point trim. They can thus replace BJT-based sensors in applications where both a wide temperature range and a high resolution are required.

#### Acknowledgments:

The authors would like to thank Zu-yao Chang for his help with the measurements, and the Advanced Packaging Center for expediting the plastic packaging.

#### References:

- [1] K. A. A. Makinwa, "Smart Temperature Sensor Survey", [Online]. Available: [http://ei.ewi.tudelft.nl/docs/TSensor\\_survey.xls](http://ei.ewi.tudelft.nl/docs/TSensor_survey.xls)
- [2] C. H. Weng et al., "A CMOS Thermistor-Embedded Continuous-Time Delta-Sigma Temperature Sensor With a Resolution FoM of 0.65 pJ/C<sup>2</sup>", *IEEE JSSC*, vol. 50, no. 11, pp. 2491-2500, Nov. 2015.
- [3] S. Pan and K. A. A. Makinwa, "A 0.25 mm<sup>2</sup>-Resistor-Based Temperature Sensor With an Inaccuracy of 0.12 °C (3 $\sigma$ ) From -55 °C to 125 °C," *IEEE JSSC*, Oct. 2018.
- [4] S. Pan et al., "A Resistor-Based Temperature Sensor with a 0.13pJ/K<sup>2</sup> Resolution FOM," *IEEE JSSC*, vol. 53, no. 1, pp. 163-174, Jan. 2018.
- [5] K. Souri et al., "A 40 $\mu\text{W}$  CMOS Temperature Sensor with an Inaccuracy of  $\pm 0.4^\circ\text{C}$  (3 $\sigma$ ) from -55°C to 200°C," *ESSCIRC*, pp. 221-224, Sept. 2013.
- [6] B. Yousefzadeh et al., "A BJT-Based Temperature Sensor with a Packaging-Robust Inaccuracy of  $\pm 0.3^\circ\text{C}$  (3 $\sigma$ ) from -55°C to +125°C After Heater-Assisted Voltage Calibration," *ISSCC*, pp. 162-163, Feb. 2017.
- [7] U. Ausserlechner et al., "Drift of Magnetic sensitivity of smart Hall sensors due to moisture absorbed by the IC-package," *IEEE Sensors*, pp. 455-458, Oct. 2004.

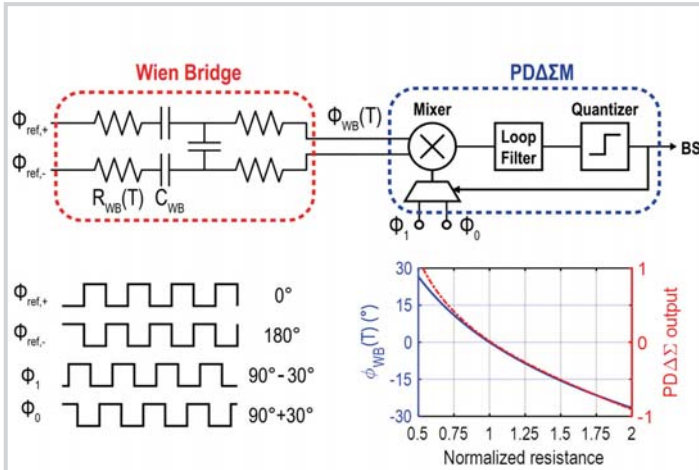


Figure 10.3.1: CTΔΣ readout of a Wien-bridge temperature sensor (top), waveforms, phase response of the Wien bridge and BS average of the PDΔΣM (bottom).

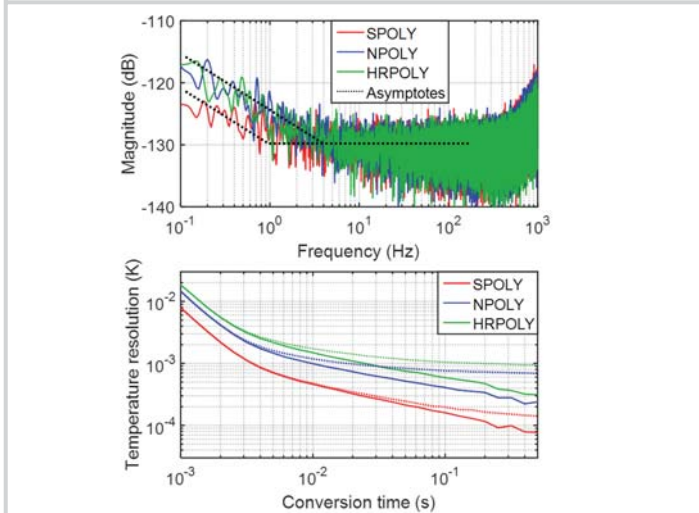


Figure 10.3.3: Bitstream spectra (100s interval, Hanning window) (top); Resolution vs. conversion time for 1s (solid lines) and 100s (dashed lines) intervals (bottom).

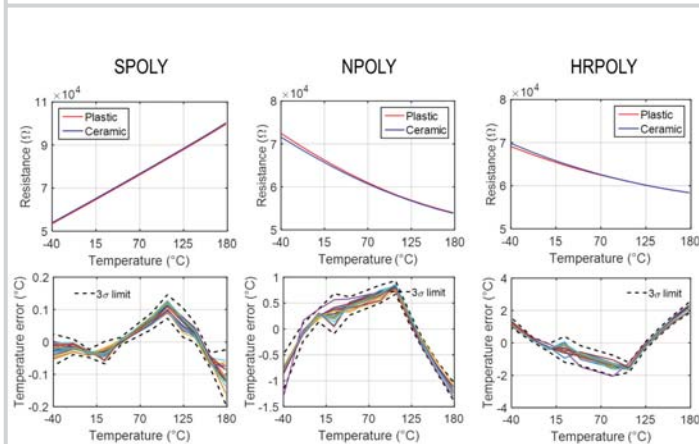


Figure 10.3.5: Average resistance vs. temperature of three types of resistors in different packages (top); Inaccuracy of plastic packaged sensors after a 1st-order fit and system non-linearity correction from ceramic packaged sensors (bottom).

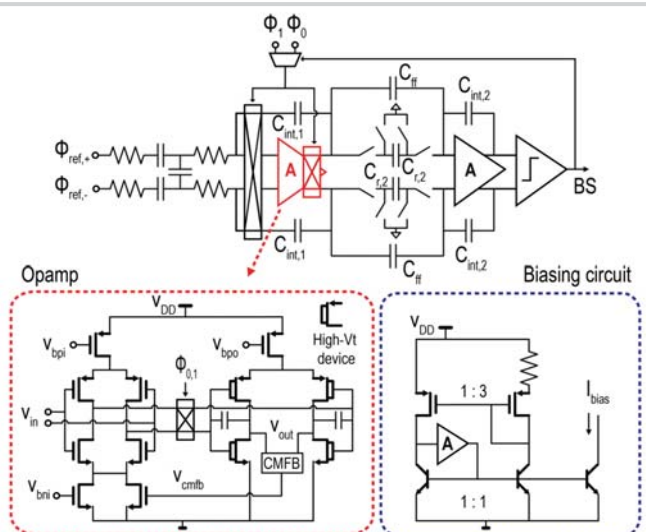


Figure 10.3.2: Block diagram of the PDΔΣM. Simplified diagram of the 1<sup>st</sup>-stage amplifier and the biasing circuit.

10

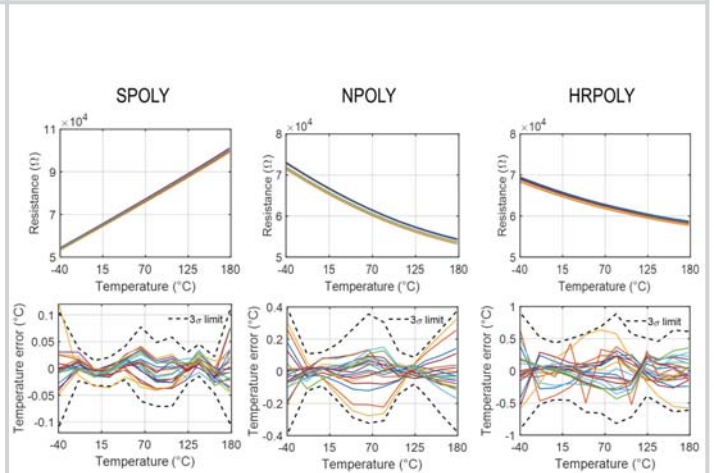


Figure 10.3.4: Extracted sensor resistance  $R_{WB}$  with ceramic packaging (top); Inaccuracy after a 1<sup>st</sup>-order fit and systematic non-linearity correction (bottom).

	[2]	[3]	[4]	[5]	This Work
Sensor type	Resistor WhB	Resistor WhB	Resistor WB	BJT	Resistor WB
Technology	0.18μm	0.18μm	0.18μm	0.16μm	0.18μm
Area [mm <sup>2</sup> ]	0.43	0.25	0.72	0.1	0.12
Temperature range	-40°C to 125°C	-55°C to 125°C	-40°C to 85°C	-55°C to 200°C	-40°C to 180°C
Trimming points	2 <sup>a</sup>	2 <sup>b</sup>	2 <sup>b</sup>	1	1   2 <sup>b</sup>
3σ inaccuracy [°C]	0.4	0.12	0.03	0.4	0.4   0.11
Relative inaccuracy	0.48%	0.13%	0.05%	0.33%	0.36%   0.10%
Supply voltage [V]	1.5	1.8	1.8	1.6	1.8
Power [μW]	65	94	160	35	52
Conversion time [ms]	0.1	5	5	4.2	10
Resolution [mK]	10	0.29	0.41	20	0.46
Resolution FoM [fJ·K <sup>2</sup> ]	650	40	130	59000	110

<sup>a</sup> 1-point trim and 1<sup>st</sup>-order fit. <sup>b</sup> 1<sup>st</sup>-order fit. <sup>c</sup> Energy / Conversion x (Resolution)<sup>2</sup>.

Figure 10.3.6: Summary of measurement results and comparison with previous work.

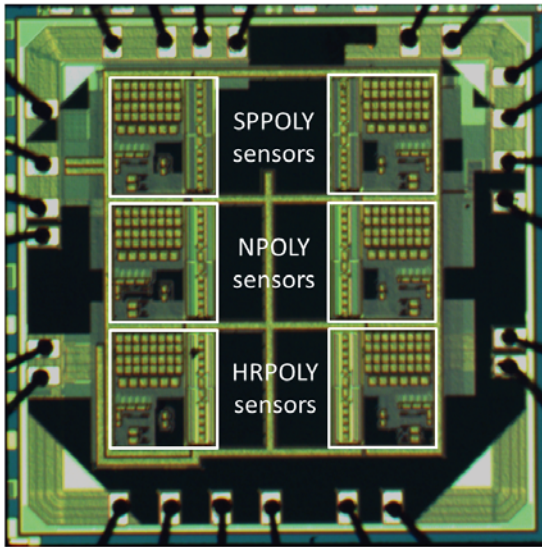


Figure 10.3.7: Micrograph of six temperature sensors on one die.